An energy description of wear mechanisms and its applications to oscillating sliding contacts

S. FOUVRY*, T. LISKIEWICZ, Ph. KAPSA, S. HANNEL, E. SAUGER

LTDS (CNRS UMR 5513), Ecole Centrale de Lyon,

36 Avenue Guy de Collongue, 69134 Ecully.

**Corresponding author S. Fouvry; Email*: siegfried.fouvry@ec-lyon.fr

Abstract: To quantify wear rates, the Archard approach is classically applied. It relates the wear volume to the product of the sliding distance and the normal load. A wear coefficient is then extrapolated and is supposed to establish the wear resistance of the studied material. This synthesis shows that this approach does not work when the friction coefficient is not constant. It appears to be much more relevant to consider the interfacial shear work as a significant wear parameter. This approach is applied to study the wear response of different steels and then extended to different hard TiN, TiC coatings under reciprocating sliding conditions. By identifying wear energy coefficients the wear quantification can be rationalized and the wear resistance of the studied tribosystems can be classified. This also appears to be a convenient approach to interpret the different wear mechanisms. Metallic materials involving plastic strain are analyzed from FEM computations. The energy balance confirms that a minor part of the dissipated energy is consumed by plasticity, whereas the major part participates in the heat and debris flow through the interface. When a load energy approach is introduced an accumulated density of the dissipated energy variable is considered to quantify the TTS (Tribologically Transformed Structure) formation. A wear ”scenario” of metallic structures is then discussed. This energy wear approach is applied to analyze hard coating wear mechanisms focusing on abrasion and oxidation phenomena. The local wear energy analysis is transposed, thus allowing the lifetime of hard coatings to be quantified.

Keywords : Fretting, wear, SC653, TiN, TiC, coating, lifetime, energy approach.

1. INTRODUCTION

Numerous experimental analyses and industrial experts’ reports conclude that fretting loadings can induce cracking or wear linked to debris formation [1, 2]. The fretting maps approach introduced by Vingsbo et al and Vincent et al have shown that the damage evolution strongly depends on the sliding regimes [3, 4]. Cracking is mainly encountered under partial and mixed fretting regimes whereas wear is observed for larger amplitudes under gross slip situations (Fig. 1). Because of research efforts of the

last 15 years, crack nucleation and the crack propagation [5, 6, 7] can now be predicted, whereas the threshold transition from a short to a long crack is in progress [8].

The situation concerning wear induced by debris formation is clearly less advanced. This is revealed by the great number of wear models and the difficulty in predicting the evolution of wear with loading parameters such as pressure, sliding velocity or friction coefficient [9]. When the contact geometry is modified, wear can also favor local overstressing and then activate cracking. In specific applications, debris induced by fretting is also prohibited.

This clearly illustrates the need to formalize wear under fretting loading and more generally for reciprocating situations. The research work developed by Godet [10] and subsequently by Berthier et al. [11] has shown that wear is a consequence of debris formation and debris ejection. To illustrate this fundamental idea, a flow chart can be drawn in which the wear rate is controlled by the balance between the flow of debris formation and debris ejection. Two extreme situations are considered to illustrate such a principle (Fig. 1b and 1c).

Some conformal contacts like the hip joint prosthesis contact or blade disk configuration tend to maintain the debris within the interface, allowing third body accommodation. Because the flow of debris ejection is low, this is what controls the wear rates and indirectly monitors the debris formation.

By contrast less conforming geometries, like sphere or cylinder/plane configurations more easily eject the debris from the interface. The contact behavior is less dependent on third body accommodation. The wear rate is then controlled more by the rate of debris formation. This latter description must nevertheless be tempered by the nature of the material of the ambient atmosphere conditions [12]. For instance, for high speed steels and hard coatings under dry or medium humidity, powder debris is formed and easily ejected from the interface (Fig.2). The present study will focus on this “non-trapping” condition by proposing a formalism for the wear.

The most common wear model proposed in tribology is the Archard model [13] which relates the wear volume to the product of the sliding distance with the normal force. A wear coefficient (K) is usually obtained from the following questions:

$$K = \frac{V}{P.S} \qquad (1)$$

with :

K : wear coefficient,

P : normal force,

S : sliding distance.

Numerous studies have shown that for a same material, the K factor and the friction coefficient strongly depend on the wear mode, displacement amplitude, contact geometry and other parameters. A recent study has shown that to predict the wear rates of metallic structures under fretting it is essential to consider the elastoplastic response of the structure. This aspect has been analyzed in depth by

Johnson [14] and Kapoor [15]. According to material hardening laws, loading conditions will maintain an elastic response, whereas, above this critical cyclic stress state, the material will undergo accumulated plastic dissipation. K.L. Johnson [14] et al. and K. Dang Van [16] defined this shakedown boundary as a function of the Hertzian pressure and the friction coefficient. A fretting wear investigation of a sintered steel with a kinematic hardening behavior under variable friction coefficient conditions has confirmed such a theory. It shows that the Archard wear coefficient increases critically when the elastic shakedown boundary is crossed (Fig.3) [17]. It shows that to quantify the wear rate under alternated sliding situations, it is essential to integrate the friction coefficient. It also underlines the limitation of the Archard model, which does not integrate such a variable in its formulation. To evaluate the intrinsic wear resistance of materials, an energy wear approach will be developed which consists in relating the material removal to the friction energy dissipated through the interface. Global and local analyses have been conducted to better understand the different damage mechanisms involved in the wear processes and to rationalize the contact durability in fretting to reciprocating sliding conditions.

2. EXPERIMENTAL CONDITIONS

2.1 Test configuration

Fretting and reciprocating tests have been conducted on a previously described MTS tension compression hydraulic system [18], and an electrodynamic shaker system (Fig. 4). The use of these two testing machines enables us to cover a wide range of normal force loadings between 50 to 500 Newtons, and displacement amplitudes from 2 to 200 µm. These two fretting wear tests are based on a similar principle where a constant normal force (P) is applied while alternating displacement is imposed (δ). The latter is recorded along with the tangential force (Q) and the normal force. The evolution of the tangential force versus displacement permits the plotting of fretting cycles. Under gross slip (or reciprocating sliding conditions), the fretting cycle displays a quadratic shape. For each cycle the maximum tangential force (Q*) and displacement (δ*) amplitudes are determined. The area of the hysteresis which corresponds to the dissipated energy is calculated (Ed). The sliding amplitude, which is different from the displacement amplitude due to the contact and apparatus compliance, is associated with the displacement value when the tangential force is zero (δ_g).

Except where specified, tests were conducted under ambient conditions at 20°C with relative humidity between 40 and 55%. After the test, the specimens were ultrasonically cleaned with alcohol, and surface profiles were obtained to measure the wear volume denoted “V” and the maximum wear depth “h”, usually observed at the center of the fretted scar.

2.2 Materials

Different materials have been studied including metals and hard coatings. Sintered steel DC1 specimens were realized from a commercial Hoganas DC1 (1.5 Mo-2.0Ni-Fe (balance)) with 0.5

carbon added. The sintering process was conducted at 1120°C during 1.5 h. A heat treatment was subsequently conducted at 930°C during 1h followed by an oil quenching. A classical hard speed steel (HSS) SC652 (0.96 at% C, 4.2 at% Cr, 5.0 at% Mo, 3.0 at% V and 6.4 at% W) was also studied. After a thermal hardening to 63 HRc, part the of the specimens were kept for the wear analysis of this steel and others used as substrate for TiN an TiC hard coatings. The studied 4 µm thick TiN coating was deposited in a Balzers triode ion plating process. The studied 4 µm thick TiC coating was obtained using a PVD magnetron sputtering process. Polycrystalline alumina and chromium steel (52100) balls, with radius 12.7 mm and a surface roughness (peak to peak) less than 0.01 µm were used as counterbodies. All the surfaces were cleaned with acetone and ethanol before the tests. The different mechanical properties of these materials are listed in the following Table1 and defined in more details in the corresponding references.

3. WEAR ENERGY DESCRIPTION

To integrate the friction coefficient in the wear analysis, the wear volume can be compared with the accumulated friction work dissipated through the interface [12, 19, 20]. This dissipated energy corresponds to the accumulated energy determined from the sum of the fretting cycle area :

$$\Sigma E_d = \sum_{i=1}^{N} E_{di} \qquad (2)$$

where E_{di} is the dissipated energy of the i^{th} cycle.

Figure 5 confirms the correlation between the wear volume extension and the dissipated energy as a function of the displacement amplitude. It can be noted that above the transition amplitude between partial and gross slip conditions a linear evolution is observed.

3.1 Wear energy analysis of metallic structure.

Figure 6a displays the wear volume versus the corresponding accumulated dissipated energy for the SC652 high-speed steel. A linear evolution is observed and an energy wear coefficient α_V can be calculated. This variable expresses the wear volume in terms of dissipated joules.

For metallic material, the linear approximation does not cross the origin but presents a small shift along the energy axis. This quantity is related to threshold energy E_{dth}, required to first transform the metallic structure before generating wear particles [17]. During the incipient loading, the surface endures severe plastic deformation which modifies the initial microstructure to a very hard phase called TTS (Tribologically Transformed Structure) [22]. This, associated with a nanocrystalline structure, will be fractured, leading to debris formation.

Therefore the wear rate is expressed by the following equation:

If $\Sigma E_d < E_{dth}$ then V=0

If $\Sigma E_d > E_{dth}$ then $V = \alpha_V.(\Sigma E_d - E_{dth})$ (3)

3.2 Wear energy analysis of ceramic coating structure.

The energy approach was extensively applied to analyze different hard coatings like PVD TiN (Fig. 6b) [19]. Figure 7 compares the different wear energy coefficient's outlining a significantly higher wear resistance of hard coatings compared to steels. Similarly it is observed that the threshold energy is lower for hard coatings than for metallic structures. This indicates that the initial plastic transformation in a metallic structure to TTS transformation is a high-energy consuming process, whereas the wear of a hard coating does not require an incubation energy to generate the first debris.

3.3 Variable amplitude conditions

The stability of the energy wear approach to predict the extent of wear was also confirmed under variable displacement amplitude conditions (VDA) [23]. Figure 8 shows the linear relationships between the wear volume and the accumulated dissipated energy independently of the displacement conditions (i.e. constant displacement amplitude conditions (CDA) or variable displacement amplitude conditions (VDA)).

4. RELATIONS BETWEEN FRICTION ENERGY AND WEAR MECHANISMS

Figure 9 illustrates how the dissipated energy can activate the different processes involved in the wear processes. This energy will participate in mechanical transformations, tribochemical phenomena, third body transformation and thermal phenomena. A question arises concerning the distribution of this energy in theses different processes.

4.1 Plastic dissipation

To estimate the quantity of energy consumed by plasticity, experimental and FEM elasto-plastic computations were compared. The modelling of the fretting cycle was conducted on an annealed CuSn4/CuSn4 cylinder (R=45 mm)/plane configuration. Cyclic tensile compressive tests were performed up to ± 10% total strain in order to determine the cyclic strain hardening behavior [24]. A Prager linear kinematic hardening law was chosen to model the material's behavior once cyclic hardening was stabilized (E=120 GPa, ν=0.34, cyclic yield stress : $\sigma_{y(cyclic)}$=200 MPa, hardening slope p=6 Gpa). The friction coefficient was experimentally determined around 0.8. Fretting cycles were modeled and compared to experimental results for ±17 µm displacement amplitude and 113 N/mm linear normal force (Fig. 10). The energy balance indicates that the proportion of energy consumed by plasticity remains small compared to the friction energy dissipated in the interface (Table 2).

The present analysis concludes that less than 10% of the energy is consumed by the plastic dissipation. More in depth investigations are nevertheless required to better consider the hardening behavior.

However this first result indicates that, even if plasticity is essential to quantify the wear of metallic structures, the energy involved in such a transformation remains relatively low.

4.2 Definition of molar wear energy

To extend the energy balance analysis of wear phenomena and permit a comparison with thermodynamical variables, a molar analysis should be considered [19]. The volumic energy wear factor can then be expressed in terms of molar energy of wear :

$$\varphi_{mol} = \frac{M}{\alpha_V . \rho} \text{ [J/mol]} \qquad (4)$$

where ρ is the density and M the molar weight.

Based on this new decription, different tribosystems tested under similar loading situations are compared in Table 3. Very high wear energies confirm the very low energy efficiency of wear mechanisms. On the other hand, a large quantity of energy needs to be dissipated to generate a relatively small quantity of wear. This comparison also confirms the higher wear resistance of the hard coating. The TiN energy of wear is at least 15 times higher than for the high speed steel SC652.

The comparison with binding energy indicates that, the stronger the atomic bonding the lower the wear energy. Indeed, the energy ratio ($\varphi_{mol} / D^{o}_{298}$) is between 10^3 for metallic structures until near 10^5 for carbide structures. The comparison with the activation energy for oxidation confirms that the higher wear performance of hard coating can partly be related to higher oxidation resistances. Nevertheless, the energy ratio (φ_{mol} / E_a) indicates that less than 0.1% of the dissipated energy participates in the oxidation process.

4.3 Synthesis

One conclusion of this energy balance investigation is that the wear process displays a ‘very poor’ energy efficiency. It also concludes that even if plasticity and oxidation play an important role in wear damage, they consume a relatively low quantity of the energy dissipated in the interface. It follows that the major dissipating processes activated in the fretted contact are heat generation and third body transformation and ejection.

5 LOCAL ENERGY ANALYSIS

The previous analysis that relates the wear volume extension to the accumulated dissipated energy appears to be a powerful means to interpret and quantify wear under fretting and extensively reciprocating sliding conditions. Nevertheless, in most situations the damage phenomena are related to length scale dimensions such as wear depth or the coating thickness before the substrate is reached. A local approach is needed, where the global energy description is derived from a local energy density analysis [20].

5.1 Explicit formulations of the dissipated energy density.

Assuming a full unidirectional sliding condition, the energy density dissipated on point M(x,y) by sliding along x for a total stroke 2.δg is deduced from the simple integration :

$$Ed_h(x,y) = \int_{-\delta_g}^{+\delta_g} q(x,y)\cdot ds = \int_{x-\delta_g}^{x+\delta_g} q(x,y)\cdot dx \quad \text{[in joule/m²]} \tag{5}$$

where q(x,y) is the shear stress field on M(x,y).

For a sphere/plane configuration, a Hertzian shear field is considered, expressed by :

$$q(x,y) = q_0 \cdot \left(1 - \frac{\left(x^2 + y^2\right)}{a^2}\right)^{1/2} \tag{6}$$

where q_0 is the maximum shear stress at the contact center defined by :

$$q_0 = \mu \cdot p_0 = \mu \cdot \frac{3\cdot P}{2\cdot \pi \cdot a^2}. \tag{7}$$

The contact radius is expressed by

$$a = \left(\frac{3\cdot P\cdot R}{4\cdot E^*}\right)^{1/3} \text{ with } \frac{1}{E^*} = \frac{1-\nu_1^2}{E_1} + \frac{1-\nu_2^2}{E_2} \tag{8}$$

and,

ν_1, ν_2 : Poisson's coefficient of the plane (1) and the sphere (2),

E_1, E_2 : Elastic Young's modulus of the plane (1) and the sphere (2).

The analysis is simplified by introducing the sliding ratio $e = \delta_g / a$. As illustrated in Figure 11, Situations where an unexposed surface is maintained at the center of the fretted surface (e<1) can be differentiated from situations where all the plane surface is exposed to the atmosphere (e>1). Figure 11b illustrates the energy density distributions as a function of the sliding ratio.

By introducing the sliding ratio "e", the determination of the maximum energy density dissipated at the center (Ed_{h0}) of the fretted scar during a cycle [20] can also be rationalized.

When e<1, $Ed_{h0} = 2\cdot q_0 \cdot a \cdot \left(e\cdot(1-e^2)^{1/2} + \arcsin(e)\right)$

When e>1, $Ed_{h0} = q_0 \cdot a \cdot \pi$ (9)

Note that for e<1, the maximum energy density is a function of the sliding ratio "e", whereas, when e>1 it remains independent of the sliding amplitude.

5.2 Definition of a transition between gross slip fretting condition and reciprocating sliding.

The energy density analysis has been extended to the more complex partial slip fretting condition. Finally, an energy density chart is introduced displaying the evolution of the maximum value of the dissipated energy as a function of the displacement amplitude (Fig. 12). It allows us to define the boundaries between the different sliding conditions.

- The partial slip condition is related to the smallest amplitudes ($\delta^* < \delta_t$) for which the contact displays an inner stick domain surrounded by a sliding annulus. The transition amplitude between partial and gross slip is expressed by Mindlin's elastic expression [25]:

$$\delta_t = \frac{\pi \cdot a}{8} \cdot \frac{q_0}{G^*} \qquad \text{with} \qquad \frac{1}{G^*} = \frac{1-\nu_1^2}{G_1} + \frac{1-\nu_2^2}{G_2} \tag{10}$$

and,

G_1, G_2 : Elastic shear modulus of the plane (1) and the sphere (2).

- Above this transition, full sliding operates through the interface that defines the gross slip fretting condition. It prevails as long as an unexposed surface is maintained through the interface and the maximum energy density increases with the displacement amplitude (e<1). The gross slip fretting condition is then related to the given expression : $\delta_t < \delta^* < \delta_t + a$ (or e=1).

-The transition toward the reciprocating sliding condition ($\delta^* > \delta_t + a$ or e>1) is then related to the condition where the whole interface is exposed to the ambient and the maximum dissipated energy density is constant and independent of the sliding stroke.

This "energy density" description of the sliding conditions means that the Running Condition Fretting Map previously introduced by L. Vincent for fretting situations can be extended to all reciprocating situations (Fig. 13). The boundaries between the partial slip and gross slip conditions and the transition between fretting and reciprocating can be plotted as a function of the displacement amplitude and the normal force.

5.3 Energy investigation of the TTS's formation.

It was shown that metallic structures enduring alternating sliding tend to generate on the top surface a specific superficial transformed layer during the very first cycles. This layer is called the Tribologically Transformed Structure or TTS (Fig. 14) [22]. Understanding the mechanisms of formation of the TTS is a key-step in the modelling of wear induced by fretting. TTS formation is considered as the first step to establish the third-body layer (powder bed) which usually separates the two contacting surfaces and in which the displacement can be accommodated. Accurate analyses of TTS have been accomplished using classical and modern analytical tools [22]. It was shown that the TTS appears as a nanocrystalline structure, corresponding to the chemical composition of the initial material and made of the more stable structure according to the equilibrium diagram. Such a structure

has an elastic Young's modulus like that of the original metallic structure, but its hardness is significantly higher and can be as high as 1000 Hv (Fig. 15).

Considering the previous remarks, it can be assumed that TTS formation is related to plastic deformation induced by the contact which generates recrystallization to a nanostructure. To quantify the kinetics of TTS formation, the TTS thickness layer measured at the center of the contact from cross section observations is compared to the corresponding accumulated dissipated energy density (i.e. the energy density at the center of the contact is calculated for each fretting cycle and integrated over the whole test duration taking into account the contact extension) (Fig. 16). A comparison between Figure 17a and 17b shows that during the incubation stage, the total depth evolution is similar to TTS, and no wear is generated. The dissipated energy only participates in the plastic transformation. At the energy threshold, the TTS layer is suddenly generated. Additional energy contributes further to damaging the TTS surface layer, generating debris and promoting wear.

The different steps of the wear processes can be quantified by using the local energy approach. The first step is initiation of the the TTS layer from plastic strain accumulation. After TTS stabilization, wear extends in depth through several fronts of progression defined first by a subsurface plastic domain, a constant TTS layer and surface wear. The TTS generation next to the plastic domain is assumed to be similar to TTS surface degradation so that the TTS thickness remains constant. This energy density approach allow us to establish an equivalent threshold energy to generate TTS which, for the studied tempered low alloy steel (35NiCrMo) is established around $5\ 10^{7}\ \mu m^{3}/J$. Considering that less than 10% of the friction energy is involved in the plastic transformation, we deduce a volumic threshold TTS activation energy around $5.10^{-8}\ J/\mu m^{3}$. This energy description means that the threshold energy of TTS can be related to the threshold energy of wear which was previously defined for metallic structures. Figure 18 illustrates how the wear 'scenario' of a metallic structure can be explained.

5.4 Prediction of the life time of surface coatings.

Another essential aspect of the present energy density approach is the ability to predict the wear depth extension. The stability of the approach is verified even under variable displacement amplitude (VDA) [23]. Figure 19, which displays the evolution of the wear depth "h" versus the accumulated energy density ΣEd_{h0}, confirms that, independently of the sliding condition (i.e. constant or variable amplitude configurations), the wear depth extension can be predicted through an equivalent energy density wear coefficient α_h :

$$h = \alpha_h \cdot \Sigma Ed_{h0} \qquad (11)$$

So how long a coating of thickness "t" will, is related to a critical energy density:

$$Ed_{hc} = \frac{t}{\beta} \quad (12)$$

This energy density description is currently being further investigated through the development of a Wohler-like energy coating lifetime prediction for solid lubricant coatings [27]. The objective is to predict the number of cycles before the substrate is reached.

This approach is applied here to a hard TiN coating for which, when the SC652 steel is reached, a friction discontinuity is observed. By noting this discontinuity, the critical number of cycles to reach the substrate "Nc" can be determined, and the life time of the coating for the studied condition defined. Figure 20a shows how the normal force and the displacement amplitude decrease the coating endurance. The description is unified by transposing the energy density approach, and relating the critical number of cycles "Nc" to the maximum energy density Ed_{h0} (Eq. 9) (Fig. 20b). This leads to a logarithmic master curve where all the results can be superimposed. By deducing a logarithm evolution, an equivalent S-N or Ed_{h0}-N curve defining the lifetime of a coating (i.e.: the number of cycles to reach the substrate as a function of the maximum energy density) (Fig. 21), can be drawn.

Further extensions will be undertaken to better analyze the wear behavior under very low and very high dissipated energy density conditions, and also to better integrate the contact extension and the decrease of the shear. However this first approach permits a very fine estimation of the lifetime of the coating over a wide spectrum of pressure and displacement amplitudes.

6. CONCLUSION

Focusing on contact situations where the third body is easily ejected from the interface, an energy wear approach, which consists of comparing the wear volume to the accumulated dissipated friction energy, has been developed. Through this synthesis work, it has been shown the following aspects:

- Taking into account the coefficient of friction, the energy approach displays a higher stability than the Archard formulation and also facilitates the analysis of wear mechanisms involved in metal and ceramic contacts. Two variables have been identified:
  - An energy wear coefficient, which relates the wear volume increase to the additional energy dissipated through the interface.
  - A threshold energy of activation, near zero for ceramic coatings, but considerable for metallic structures, which corresponds to the incipient energy required to plastically transform the metal to TTS.
- By extending this approach through the introduction of molar wear energy variables, the comparison between surface treatments has been rationalised. More in-depth investigations based on an energy balance analysis conclude that, even through the friction energy appears to be an activating factor of wear phenomena, plastic transformations and oxidation seems to be processes

which consume little. Most of the energy is assumed to be consumed by thermal dissipation and through the third body transformations.

To more precisely study the wear phenomena and predict the surface treatment lifetimes, an energy density description has been derived. Simple analytical formulations have been introduced to calculate the maximum energy density dissipated per cycle as a function of the sliding amplitude.

- The boundary between the different sliding domains can be quantified and a rational definition of the transition between fretting and reciprocating sliding given.
- Transposing this local energy description to analyze wear mechanisms showed that it could quantify the TTS's formation. A threshold energy of TTS generation has been identified for a low alloyed steel, which could also be related to a critical plastic work density. Below this energy, the microstructure is unchanged and above this density, the metallic microstructure is transformed to TTS.
- Applied to hard coating tribosystems, the energy density approach permits the quantification of the wear depth extension, so the surface treatment lifetime can be predicted. This approach has been validated for constant but also variable amplitude conditions for a TiC/alumina contact. It was also applied to predict when TiN/alumina contacts under high pressure and displacement amplitude conditions would wear through. It permits the introduction of an equivalent Wear-Energy chart. The number of fretting or reciprocating cycles applied to reach the substrate is related to the maximum value of the energy density dissipated through the interface. Formalizing the contact endurance, this energy density description allows the introduction of a $Ed_{h0} - N$ diagram by analogy to the classical fatigue S-N curve. This analysis, allowing a more relevant comparison between surface treatments, is currently extended to better integrate the contact geometry evolution induced by wear and to interpret wear mechanisms activated under low and high friction energy density conditions.

References :

[1] R.B. Waterhouse, *Fretting Fatigue*, Applied Science publishers, (1981).

[2] D. Hoeppner, “Mechanisms of fretting fatigue and their impact on test methods development” ASTM STP 1159, 1992, pp. 23-32.

[3] O. Vingsbo, S. Soderberg, “On fretting maps”, Wear, 126 (1988), p. 131-147.

[4] L. Vincent, Y. Berthier, M. Godet, “Testing methods in fretting fatigue: a critical appraisal” ,ASTM STP 1159, 1992, p. 33-48.

[5] D. Nowell, D.A. Hills, “Testing methods in fretting fatigue: a critical appraisal”, Wear, 136, (1990), p. 329 - 343.

[6] S. Fouvry, Ph. Kapsa, L. Vincent, K. Dang Van, "Theoretical analysis of fatigue cracking under dry friction for fretting loading conditions", Wear, 195 (1996), p. 21-34.

[7] T.N. Farris, M.P. Szolwinski, G. Harish, “Fretting in Aerospace Structures and Materials”, ASTM STP 1367, 2000, p.523-537.

[8] M. Dubourg and V. Lamacq, “Stage II Crack Propagation Direction Under Fretting Fatigue Loading: A New Approach in Accordance with Experimental Observations”, ASTM STP 1367, (2000), p. 436.

[9] H.C. Meng, K.C. Ludema, “Wear models and predictive equations : their form and content” ,Wear 181 - 183, (1995), p. 443-457.

[10] M. Godet, “The third body approach, a mechanical point of view of wear”, Wear ,100, (1984), p. 437-452.

[11] Y. Berthier, L.Vincent, M. Godet, ”Velocity accommodation in fretting”, Wear, 125, (1988), p. 25-38.

[12] H. Mohrbacher, B. Blanpain,J.P. Celis, J.R. Roos, “ Oxidational wear of TiN coating on tool steel and nitrided tool steel in unlubricated fretting”, Wear, 180, (1995), p. 43-52.

[13] F. Archard,J. , “Contact and rubbing of flat surfaces”, Appl. Phys., 24 (1953), p. 981-988.

[14] K.L. Johnson, “Contact mechanics and wear of metals”, Wear, vol. 190 (1995), p. 162-170.

[15] A. Kapoor, “Wear by plastic ratchetting”, Wear 212 (1997), p. 119-130.

[16] K. Dang Van, M.H. Maitournam, “Elasto-Plastic Calculations of the Mechanical State in Reciprocating Moving Contacts: Application to Fretting Fatigue”, ESIS 18, (1994), Mechanical Engineering Publications, London, p. 164-168.

[17] S. Fouvry, Ph. Kapsa, L. Vincent, “An elastic plastic shakedown analysis of fretting wear”, , Wear 247, 2001, p. 41-54.

[18] C.Colombié, Y. Berthier, A. Floquet, L. Vincent and M. Godet, “Fretting: Load carrying of wear debris”, ASME Trans., 106, (1984).

[19] S. Fouvry, Ph. Kapsa, "An Energy Description of Hard Coatings Wear Mechanisms”, Surface & Coating Technology, 138 (2001) p.141-148.

[20] S. Fouvry, Ph. Kapsa, H. Zahouani, L. Vincent, "Wear analysis in fretting of Hard coatings through a dissipated energy concept", Wear 203-204 (1997), p. 393-403.

[21] R.C. Bill, ASLE transactions, “Steel and selected fretting-resistance surface treatments”,Vol. 21, 3, (1977), p.236-242.

[22] E. Sauger, S. Fouvry , L. Ponsonnet, J.M. Martin , Ph. Kapsa, L., Vincent “Tribologically Transformed Structure in Fretting”, Wear 245, 2000, p.39-52.

[23] T. Liskiewicz, S. Fouvry, B. Wendler, “Impact of variable loading conditions on fretting wear”, Surface and coating technology”, N° 163-164, (2003), p. 465-471.

[24] S. Hannel, S. Fouvry, Ph. Kapsa, L. Vincent, “The fretting sliding transition as a criterion for electrical contact performance”, Wear 249 (2001) p.761-770.

[25] R.D. Mindlin, H. Deresiewicz, “Elastic spheres in contact under varying oblique forces”, ASME Trans, Serie E, Journal of Applied Mechanics, 20, (1953), p. 327-344.

[26] C. Langlade, B. Vannes., M. Taillandier,P. Pierantoni, “Fretting behavior of low-friction coatings: contribution to industrial”, Tribology International 34 (2001) 49.

[27] V. Fridrici, S. Fouvry, Ph. Kapsa, Ph. Perruchaud, submitted to Tribology Letters.

TABLES

Table 1: Mechanical properties of the studied materials.

	E(GPa) Young's modulus	ν Poisson Coefficient	H Hardness
Alumina (counterbody)	370	0.27	2300 Hv
52100 (counterbody)	210	0.3	740 Hv
HSS (SC652)	230	0.28	800 Hv
DC1 (sintered steel) [17]	200	0.3	370 Hv
TiN(4µm)-(SC652 substrate) [19]	330	-	2200 Hv
TiC(4µm) -(SC652 substrate)	450	0.2	2500 Hv

Table 2 : Numerical energy balance of the stabilized fretting cycle (experimental dissipated energy : 15.5 mJ)

Energy balance of the fretting cycle	Total dissipated energy Ed(mJ)	Friction dissipation Ef (mJ)	Plastic dissipation Ep (mJ)	Ep/Ef (%)
Numerical results	16.89	15.82	1.02	7.4

Table 3 : Friction, Archard and Energy wear parameters defined from the studied tribosystems (R² : regression coefficient, E_a energy activation for oxidation, D^{o}_{298}, binding energy*).*

	metallic structures		carbide and nitride	
	DC1	SC653	TiN	TiC
$\alpha_V\ (mm^3/J)$ (R^2)	$56\ 10^{-6}$ (0.86)	$26\ 10^{-6}$ (0.95)	$2.7\ 10^{-6}$ (0.95)	$5\ 10^{-7}$ (0.90)
$Ed_{th}(J)$	57	14	2.3	0
$M(g/mole)$	56	56	62	60
$\rho(g/mm^3)$	$7.9\ 10^{-3}$	$7.9\ 10^{-3}$	$5.4\ 10^{-3}$	$4.9\ 10^{-3}$
$\varphi_{mol}\ (kJ/mol)$	$0.13\ 10^{6}$	$0.28\ 10^{6}$	$4.2\ 10^{6}$	$24\ 10^{6}$
$D^{\circ}_{298}(kJ/mol)$	75	75	476	423
$\frac{\varphi_{mol}}{D^{\circ}_{298}}$	1700	4000	9000	56000
$E_a\ (kJ/mol)$			$TiN \Rightarrow TiO_2$ 246	$TiC \Rightarrow TiO_2$ 192

FIGURE CAPTION

Figure 1 : Flow chart illustrating the third body wear approach; (a) :balance between debris formation and ejection flow, (b) : Wear rates controlled by debris ejection, (c) : Wear rates controlled by debris formation.

Figure 2 : SEM observation of a TiC/alumina fretting wear scar (most debris is ejected).

Figure 3 : Wear map of the DC1/alumina contact under gross slip fretting wear taking into account the shakedown behavior [17] : —: elastic limit (Von Mises); ▬: elastic shakedown limit for repeated sliding (kinematic hardening); ■: High wear regime $16000<K(\mu m^3/N.m)<38000$, □: Low wear regime $K(\mu m^3/N.m)<3000$ (p_0 : maximum Hertzian pressure; k : shear yield stress).

Figure 4 : Illustration of the experimental fretting wear approach : (a) diagram of the electrodynamic fretting rig, (b) analysis of the fretting cycle (determination of the loading variables).

Figure 5 : Normalized evolutions of the wear volume (AISI 9310/9310, f=163 Hz, P=1.47 N, dry air, [21]) and the dissipated energy versus the displacement amplitude. The reference point corresponds to the sliding transition between partial and gross slip ($Vt=10^{-5}$ mm^3, $\delta t= 16.5$ µm).

Figure 6 : Energy analysis of fretting wear (P : 50-200N, δ*: 25-200µm, RH : 50%): identification of the energy wear factor α_V and the threshold energy of activation E_{dth} [19]: (a) SC652/alumina, (b) TiN/alumina.

Figure 7 : Evolution of the energy wear factors and threshold energy of the studied materials.

Figure 8 : Energy wear analysis of the TiC/alumina contact (P=100N, RH=50%, N=5000-25000 cycles, f=5Hz), Linear correlation between the wear volume (V) and the accumulated dissipated energy E_{dth} (CDA: constant displacement amplitude, VDA: variable displacement amplitude).

Figure 9 : Schematic illustration of the energy partition and the activation of the various damage mechanisms involved in wear.

Figure 10 : (a) Illustration of the FEM computation of the CuSn4 cylinder/plane contact, (b) Comparison between the experimental and numerical fretting cycles.

Figure 11 : (a) Definition of the sliding ratio “e”, (b) Energy density distributions as a function of the sliding ratio.

Figure 12 : Definition of the sliding conditions as a function of the maximum energy density evolution: (a) transition between partial and gross slip, (b) transition between fretting and reciprocating.

Figure 13 : Generalized Running Condition Fretting Map (SC652/100C6, R=12.7mm).

Figure 14: Cross section observation of TTS (35NiCrMo).

Figure 15 : Microhardness of various materials [24]; ❑ Original material, ▨ TTS.

Figure 16 : Correlation between the density energy analysis and the parameters characterizing the transformation within the fretting scar, Z_{TTS} : thickness of the TTS, Z_U : Wear depth, Z_T : total transformed layer below the contact.

Figure 17 : Evolution of the TTS (a) and the total thickness (b) of a low alloy steel (35NiCrMo) versus the accumulated dissipated energy density [22]: ☐: different number of cycles, ○ : different displacements, ◆ : different normal forces.

Figure 18 : Schematization of the wear process through the energy approach: Initial energy of activation is required to transform the surface layer (TTS) before generating debris formation.

Figure 19 : Evolution of the wear depth extension (TiC/alumina) as a function of the accumulated energy density (the loading conditions are referred in Fig. 8).

Figure 20 : Illustration of the lifetime approach of a coating under fretting loading condition (TiN(4µm)/alumina (R=12.7 mm), RH=50%, f=5 Hz, ◆ : P=50 N, ☐ : P=100 N, ● : P=150 N) : (a) : evolution as a function of the displacement amplitude, (b) : evolution as a function of the dissipated energy density.

Figure 21: Introduction of the Ed_{h0}-N curve defining the endurance of TiN (4µm) /alumina contact under fretting contact (defined from Fig. 20: δ*= 50-200µm, RH=50%, f=5 Hz, ◆ : P=50 N, ☐ : P=100 N, ● : P=150 N).

FIGURES

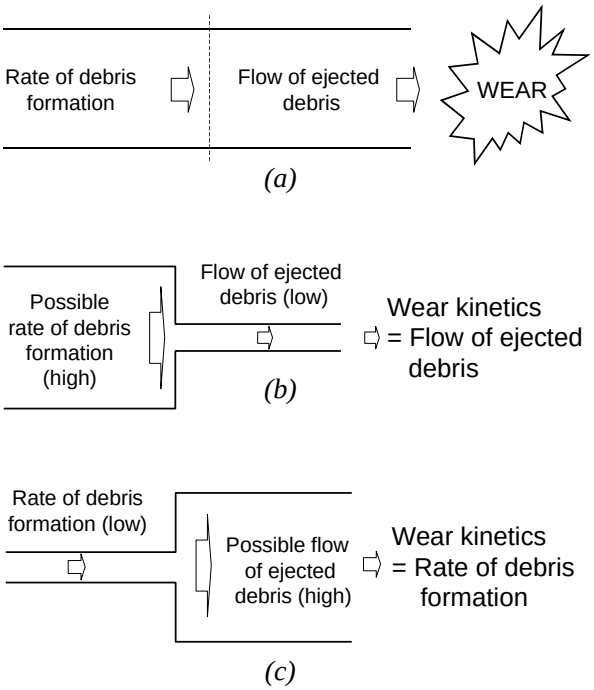

Figure 1

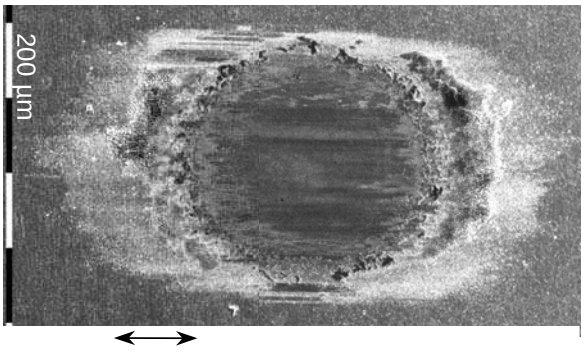

Figure 2

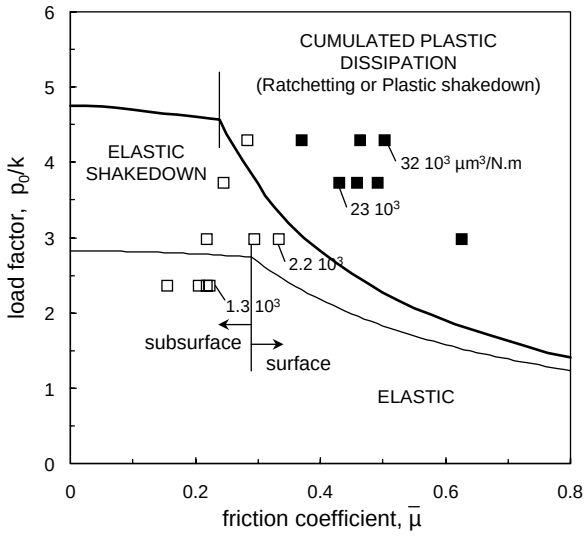

Figure 3

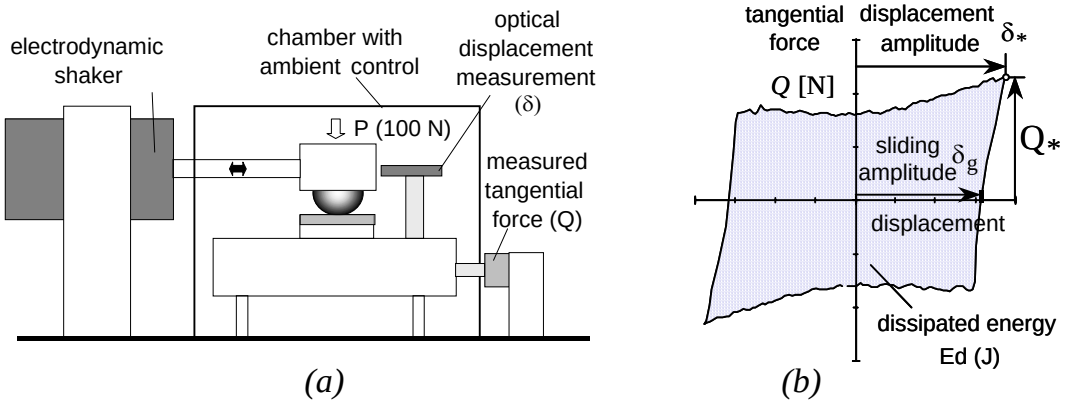

(a) *(b)*

Figure 4

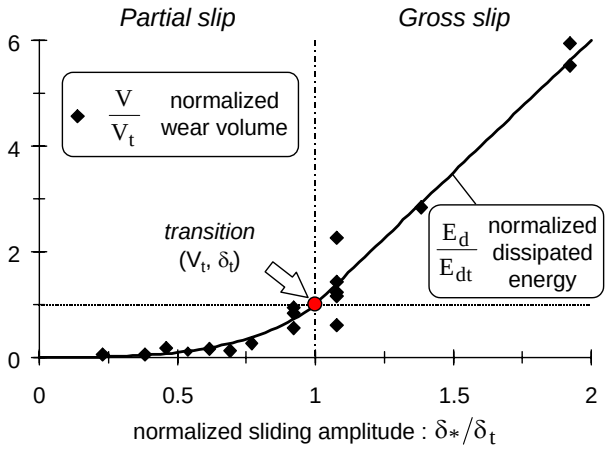
Partial slip
Gross slip
6
4
2
0
0
0.5
1
1.5
2
V / Vt
normalized wear volume
transition
(Vt, δt)
Ed / Edt
normalized dissipated energy
normalized sliding amplitude : δ* / δt

Figure 5

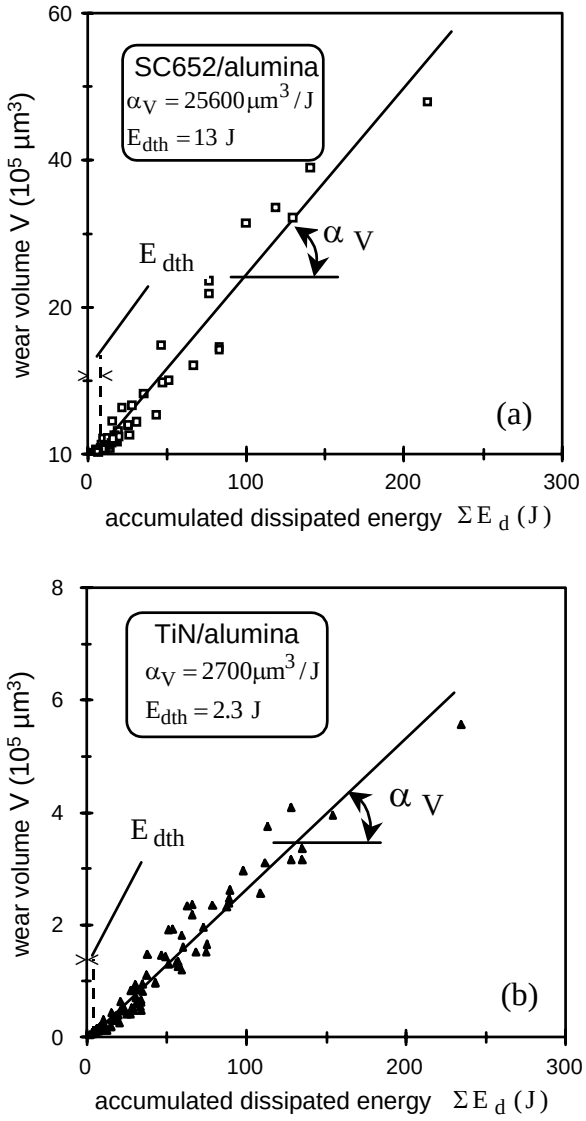
SC652/alumina
$\alpha_V = 25600 \mu m^3/J$
$E_{dth} = 13$ J
E_{dth}
α_V
(a)
wear volume V (10^5 µm³)
accumulated dissipated energy ΣE_d (J)
TiN/alumina
$\alpha_V = 2700 \mu m^3/J$
$E_{dth} = 2.3$ J
E_{dth}
α_V
(b)
wear volume V (10^5 µm³)
accumulated dissipated energy ΣE_d (J)

Figure 6

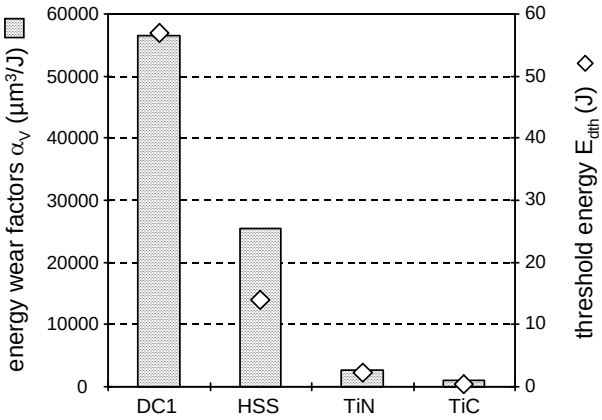

Figure 7

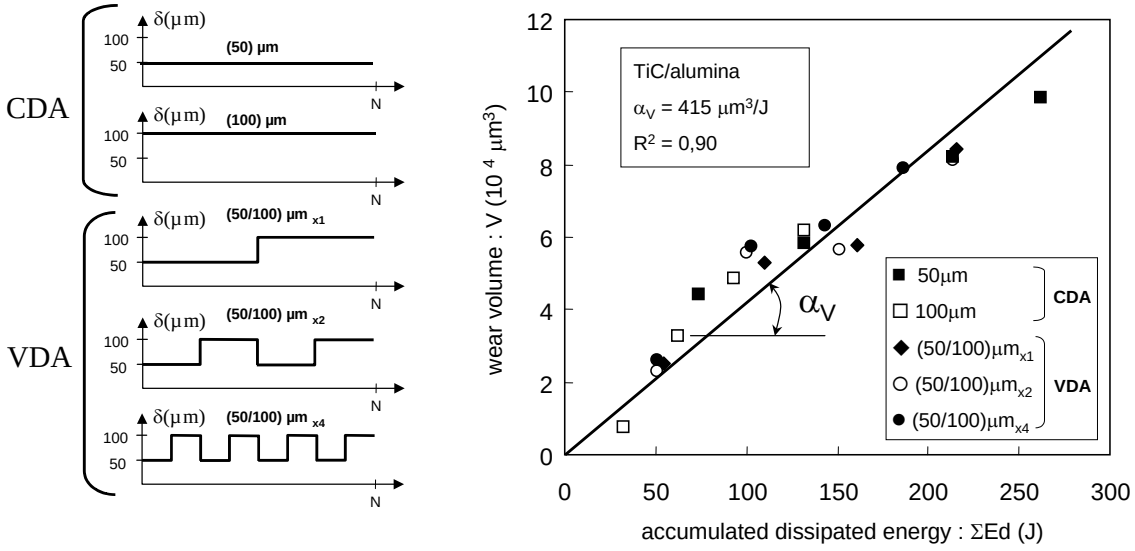

Figure 8

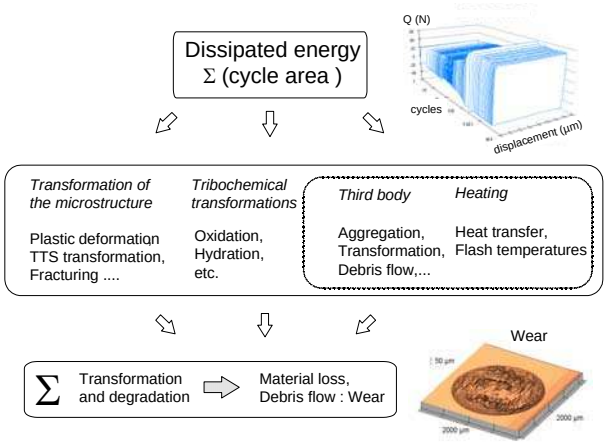

Figure 9

FEM modelling (CuSn4/CuSn4)

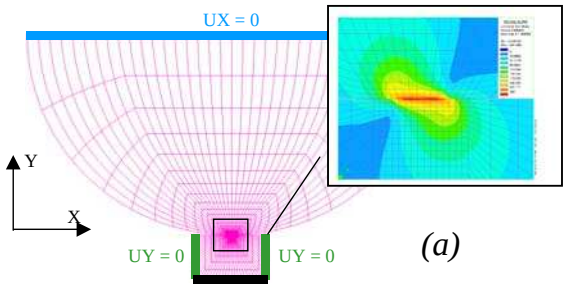

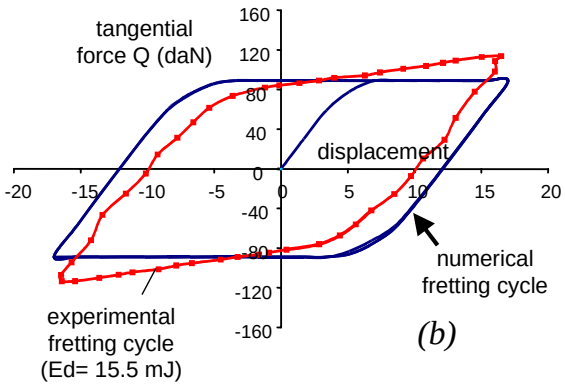

Figure 10

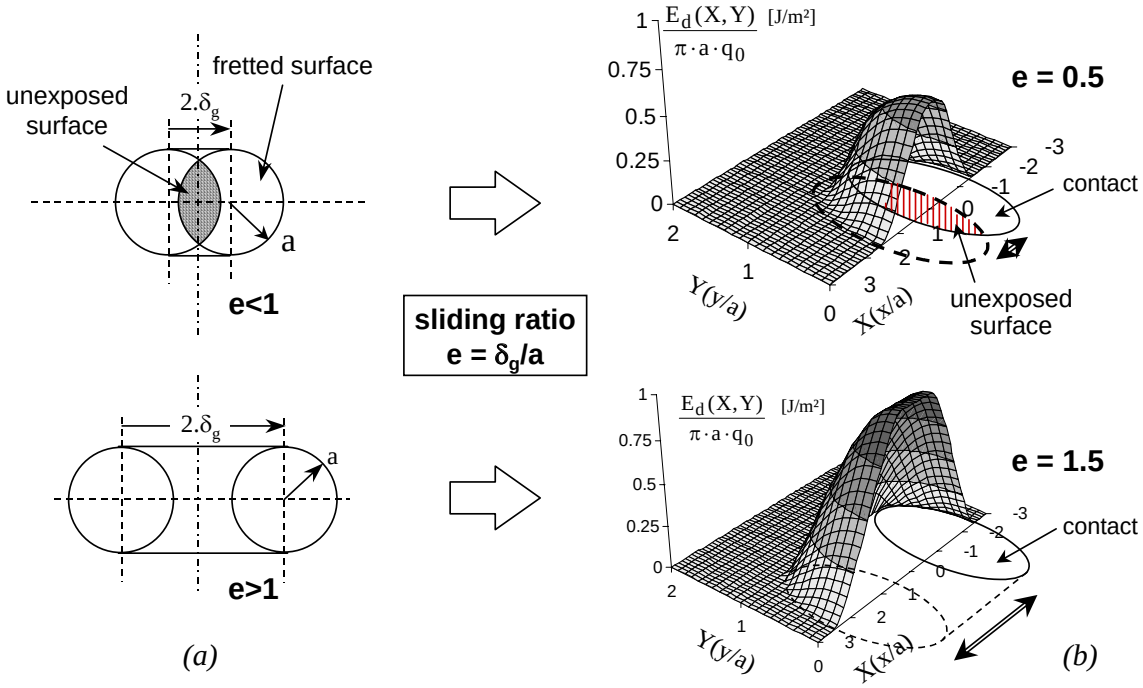

Figure 11

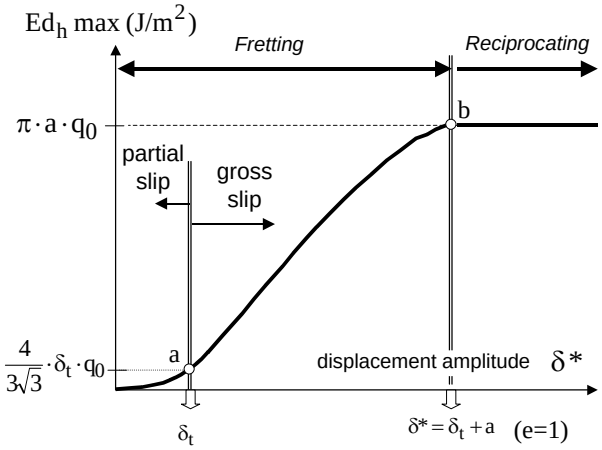

Figure 12

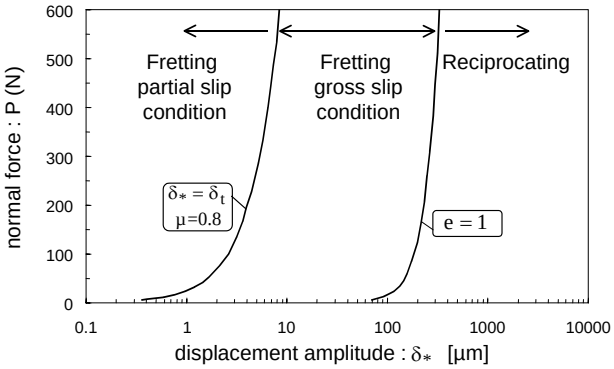

Figure 13

Figure 14

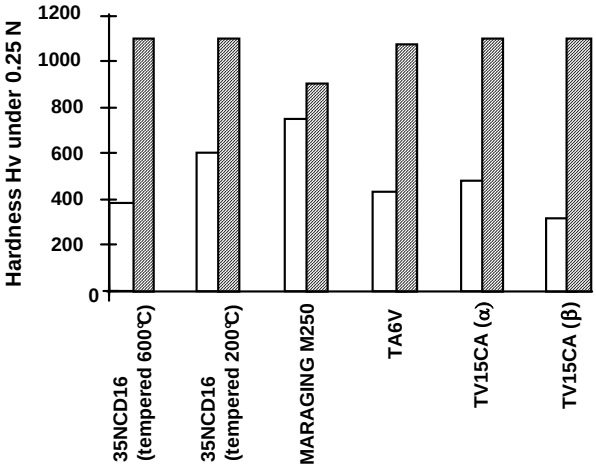

Figure 15

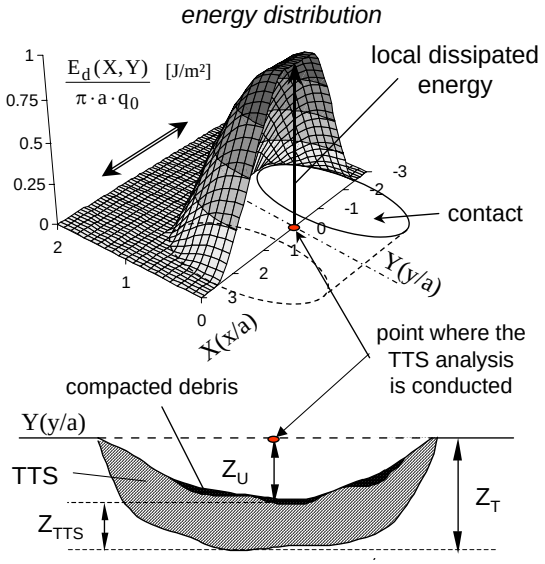

Figure 16

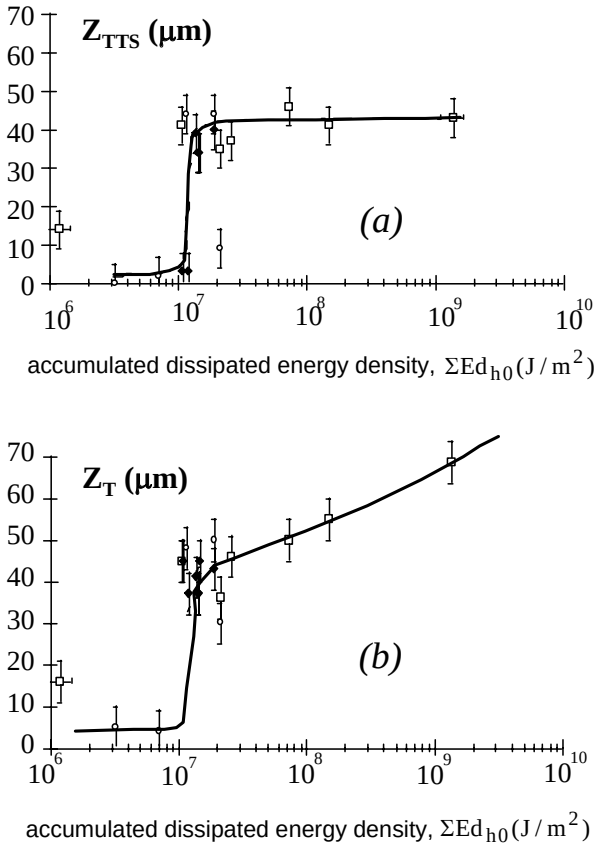

Figure 17

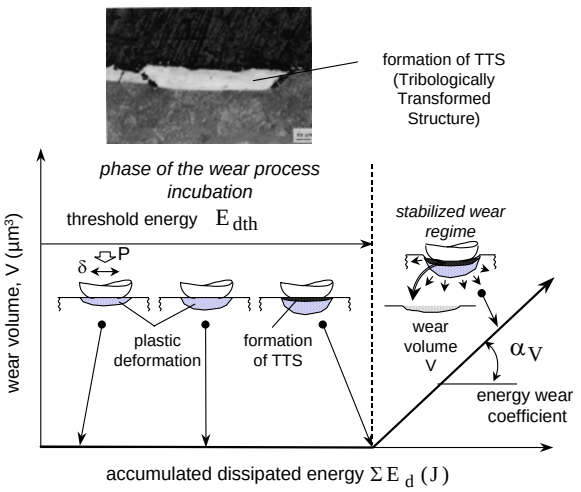

Figure 18

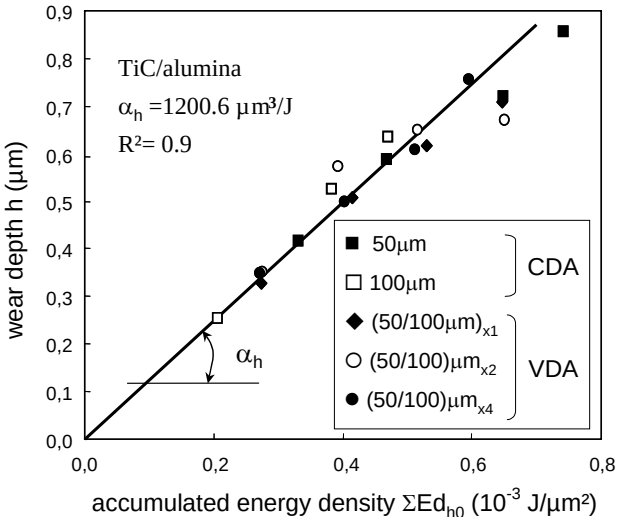
TiC/alumina
α_h =1200.6 µm³/J
R²= 0.9
wear depth h (µm)
accumulated energy density ΣEd$_{h0}$ (10^{-3} J/µm²)
50µm
100µm
CDA
(50/100µm)$_{x1}$
(50/100)µm$_{x2}$
(50/100)µm$_{x4}$
VDA
α_h
0,0
0,1
0,2
0,3
0,4
0,5
0,6
0,7
0,8
0,9
0,0
0,2
0,4
0,6
0,8

Figure 19

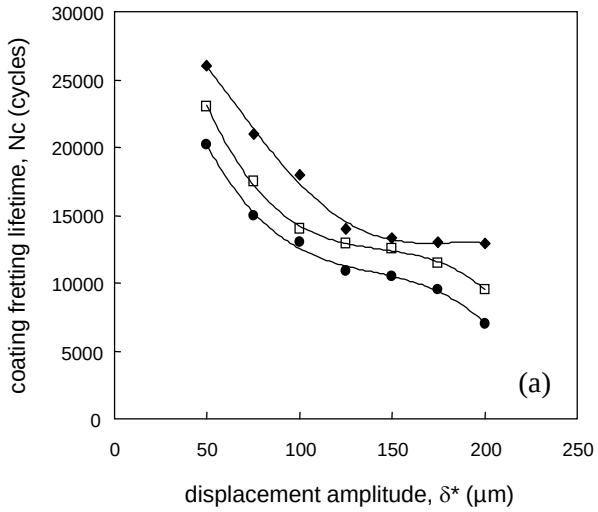
30000
25000
20000
15000
10000
5000
0
coating fretting lifetime, Nc (cycles)
0
50
100
150
200
250
displacement amplitude, δ* (µm)
(a)

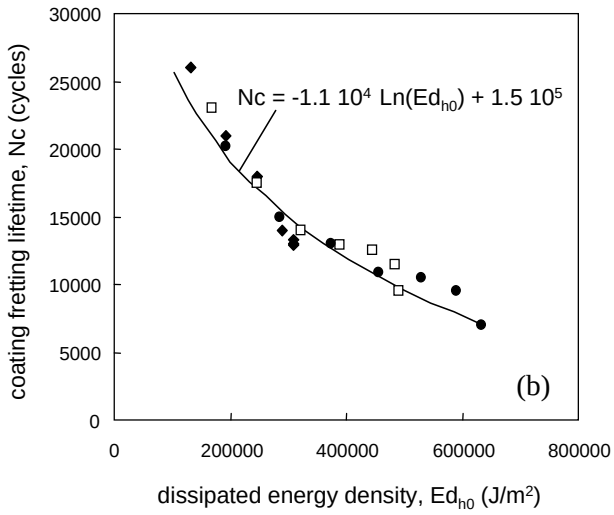
30000
25000
20000
15000
10000
5000
0
coating fretting lifetime, Nc (cycles)
Nc = -1.1 10⁴ Ln(Edh0) + 1.5 10⁵
0
200000
400000
600000
800000
dissipated energy density, Edh0 (J/m²)
(b)

Figure 20

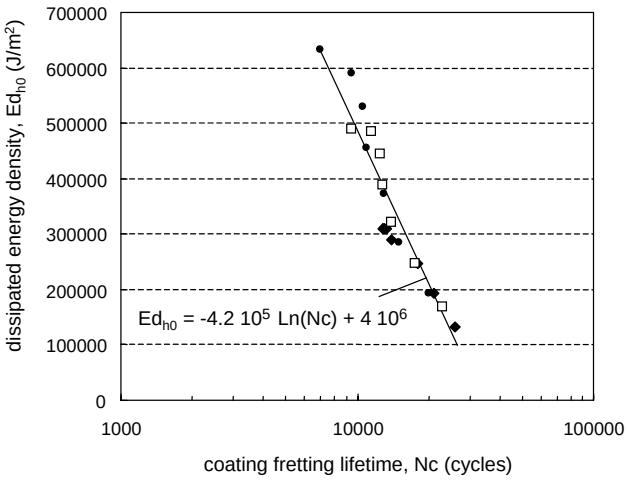
700000
600000
500000
400000
300000
200000
100000
0
dissipated energy density, Ed$_{h0}$ (J/m^2)
Ed$_{h0}$ = -4.2 10^5 Ln(Nc) + 4 10^6
1000
10000
100000
coating fretting lifetime, Nc (cycles)

Figure 21